INTERFACE

rsif.royalsocietypublishing.org

Research

Cite this article: Lenz PH, Takagi D, Hartline DK. 2015 Choreographed swimming of copepod nauplii. *J. R. Soc. Interface* **12**: 20150776.
http://dx.doi.org/10.1098/rsif.2015.0776

Received: 29 August 2015
Accepted: 30 September 2015

Subject Areas:
biomathematics, environmental science

Keywords:
Crustacea, inertia, viscosity, Stokes flow, paddle, propulsion

Author for correspondence:
Petra H. Lenz
e-mail: petra@pbrc.hawaii.edu

Choreographed swimming of copepod nauplii

Petra H. Lenz[1], Daisuke Takagi[2] and Daniel K. Hartline[1]

[1]Békésy Laboratory of Neurobiology, Pacific Biosciences Research Center, University of Hawaii at Manoa, 1993 East West Road, Honolulu, HI 96822, USA
[2]Department of Mathematics, University of Hawaii at Manoa, 2565 McCarthy Mall, Honolulu, HI 96822, USA

PHL, 0000-0002-2460-5464

Small metazoan paddlers, such as crustacean larvae (nauplii), are abundant, ecologically important and active swimmers, which depend on exploiting viscous forces for locomotion. The physics of micropaddling at low Reynolds number was investigated using a model of swimming based on slender-body theory for Stokes flow. Locomotion of nauplii of the copepod *Bestiolina similis* was quantified from high-speed video images to obtain precise measurements of appendage movements and the resulting displacement of the body. The kinematic and morphological data served as inputs to the model, which predicted the displacement in good agreement with observations. The results of interest did not depend sensitively on the parameters within the error of measurement. Model tests revealed that the commonly attributed mechanism of 'feathering' appendages during return strokes accounts for only part of the displacement. As important for effective paddling at low Reynolds number is the ability to generate a metachronal sequence of power strokes in combination with synchronous return strokes of appendages. The effect of feathering together with a synchronous return stroke is greater than the sum of each factor individually. The model serves as a foundation for future exploration of micropaddlers swimming at intermediate Reynolds number where both viscous and inertial forces are important.

1. Introduction

Aquatic microorganisms inhabit a world dominated by viscous forces, a world where the physics of swimming differs from that of macroorganisms [1,2]. The strategy used by the most numerous aquatic metazoans operating at low Reynolds number (*Re*) is to swim by paddling, which involves the repeated back-and-forth movement of one or more pairs of swimming appendages in a pattern of alternating power and return strokes. However, a rigid paddle moving back and forth at low *Re*, regardless of velocity variations, performs 'reciprocal motion', known to be incapable of net forward progress [3]. Nevertheless, nauplii can and do swim quite effectively, some with velocities ranging over two orders of magnitude, achieving maxima of over 500 body-lengths per second. How do these micro-paddlers manage to swim so fast?

The generally accepted answer is that the surface area of a swimming appendage normal to the direction of its motion is modified during different phases of the swim cycle, being maximized during power strokes and minimized during return strokes by 'feathering', to decrease drag [4–9]. However, it is unclear whether the full forward motion of an organism paddling with more than one pair of swimming appendages depends on the same principle, and many small crustaceans swim by means of the coordinated beating of two or more pairs [5,10–12]. Recent models of crustacean swimming have incorporated the phase relations between adjacent appendages as well as inertia to compute the net force on the body during distinct power and return strokes [13–15]. These models incorporate either the inertia of the swimmer or that of the surrounding fluid flow (but not both). This introduces several fitting parameters that in turn introduce uncertainty about model validity. At *Re* well below 1, free parameters can be reduced, because accurate models can then be based on Stokes flow, ignoring inertia. To

THE ROYAL SOCIETY PUBLISHING

procure data on locomotion in this range, we have used one of the smaller paddling microswimmers available, the nauplii of the paracalanid copepod *Bestiolina similis* (length 70–200 µm) [16,17]. Nauplii of this size swim at *Re* of 0.1–10 [18], which is thus transitional between low and intermediate *Re*. Simplifications that have minimal impact on predictions can allow direct measurement of the morphological and kinematic parameters needed for modelling, so none are free. A relatively simple mathematical description is then applied that can be confined to the measured quantities, without sacrificing predictive capability. The purpose is to determine how well such a simplified model succeeds in accounting for observed swimming behaviour. As *Re* increases into the transition zone, deviations are expected to develop, providing new insights into swimming at intermediate *Re* where viscous and inertial forces are important. The minimal model we have employed is based on slender-body theory for Stokes flow adapted from one that was recently developed by one of us [19]. It differs from previous models in not relying on any net force or inertia for propulsion. By accounting individually for the empirically measured dimensions and kinematics of all six paddling appendages, our model was used to predict displacements of the body over time and compare these results with direct observations to assess the neglected effects of inertia. In addition, the vetted model was used to quantify the contribution to displacement of each appendage pair, feathering of setae and appendage stroke phase in order to better understand their role in naupliar propulsion.

2. Material and methods

2.1. High-speed videography of naupliar swimming

High-resolution measurements of angular position of individual appendages and body displacement were made for nauplii of *B. similis*. Nauplii were obtained from cultures maintained in the laboratory for less than 1 year under standard conditions as described in VanderLugt & Lenz [20]. Briefly, *B. similis* adults were isolated from mixed plankton collections from Kaneohe Bay Island of Oahu, Hawaii, and cultured at ambient temperature (24–28°C), a 12 L : 12 D light regime, and fed ad libitum with live phytoplankton (*Isochrysis galbana*). Experimental nauplii were isolated from the cultures and identified to stage using morphological characteristics and length and width measurements [17].

For videography, nauplii were placed into small Petri dishes (35 mm diameter) at ambient food levels. Experimental nauplii ranged in size from 70 to 150 µm corresponding to developmental stages NI to NV. Spontaneous fast swims were recorded at 5000 fps with a high-speed video system (Olympus Industrial *i-SPEED*) filmed through an inverted microscope (Olympus IX70) with a 10× objective. Frames of the video files were converted into bitmap image files ('tiff' format) and analysed using ImageJ (Wayne Rasband; web page: rsbweb.nih.gov/ij/). Six swim episodes were analysed for appendage angles and location over multiple power/return stroke cycles at 0.2 ms intervals. The angle of each appendage was measured using the main axis of the nauplius as a reference, as shown in a scanning electron micrograph of an early nauplius (NI) in figure 1*a*. Location was determined by tracking the *x*- and *y*-coordinates of the anterior medial margin of the head in each successive frame during the swim sequence. Five additional swim episodes were analysed for location during rapid swims to determine forward, backward and net displacements. Swims were usually initiated from rest (figure 1*b*), which was characterized by a stereotypical position for each appendage: first antenna (A1) pointing anteriorly (6–12°), the second antenna (A2) pointing mostly laterally (60–90°) and the mandible (Md) posteriorly (105–135°).

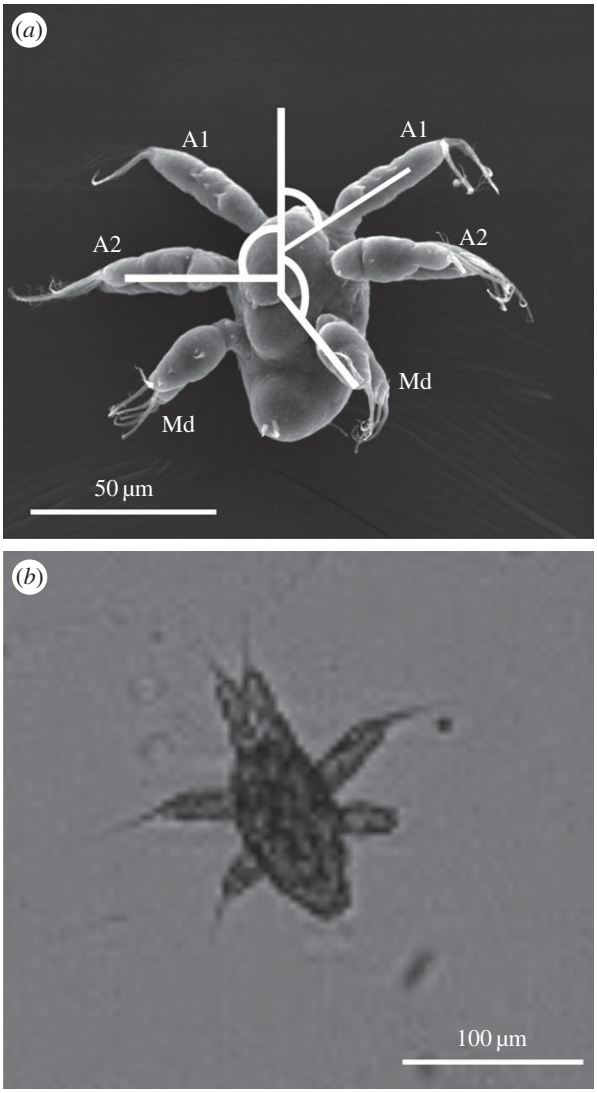

Figure 1. *Bestiolina similis* nauplii. (*a*) Scanning electron micrograph of a first nauplius (NI) showing angle measurements for first antenna (A1), second antenna (A2) and mandible (Md). (*b*) Nauplius stage 3 (NIII) video image showing position of appendages at rest. Scanning electron micrograph courtesy of Jenn Kong. Appendage abbreviations, A1, A2 and Md, used in all figures.

2.2. Model formulation

To determine the extent to which observed locomotion of a nauplius could be accounted for based on observed appendage movements and the assumptions of a low *Re* regime (see Introduction), we employed a model of swimming with rigid appendages adapted from one based on slender-body theory for Stokes flow [19]. The aim of the model is to predict the position of the body, as the angle of each leg changes over time. The model provides us a reasonable approximation for long and slender appendages paddling at low *Re* [21], which omits inertia, as explained in the Introduction. It makes several additional simplifying assumptions intrinsic to its formulation. The copepod nauplius has a compact rounded body (figure 1) that is simplified in the model as a sphere with a diameter that is the mean of the length and width of its body. Using the more accurate prolate ellipsoid shape instead made little difference in predicted displacements. Naupliar appendages are relatively rigid elongate rods, slightly tapering at both ends, again with rounded cross section. In the model, they were simplified and represented as uniform cylinders, with a single diameter. While the appendages are only an order of magnitude greater in length compared with their thickness, for the

sake of simplicity, the swimmer is modelled as a sphere with extremely slender cylindrical legs that extend radially outwards, using mean diameters measured from micrographs.

Movement of the nauplius is computed as a balance between forces propelling it through the medium and the drag resisting that movement. Linearity at low *Re* and the slenderness of the appendages (the assumption that the legs do not interact hydrodynamically) make it possible to decompose the total force on the swimmer into three parts: the 'propulsive' part, which is proportional to the angular velocity of the legs, and two drag parts proportional to the translational velocity of the nauplius, one on the fixed legs and one on the spherical body. Separate expressions derived for these forces can then be equated and solved for the velocity of the nauplius. This is fundamentally different from computing drag on a surface in a flow at high *Re*, which typically scales as the square of the fluid velocity relative to the surface. While each leg may experience some force as it moves through the fluid, there is no net force exerted on a neutrally buoyant swimmer at low *Re*. Thus, briefly (see Takagi for a more rigorous treatment [19]), for a series of legs, i, of length L_i and very much smaller diameter d_i ($d_i \ll L_i$) extending from a sphere of radius R and pivoting at its centre, each small leg segment, dr, located at a distance, r, from the pivot, moves with a velocity $r\,\dot{\theta}$. Its contribution to propulsive force directed parallel to the forward axis is the product of a constant, k, multiplied by the segment velocity, the segment length and the sine of the angle the leg makes with the axis where $df_{\mathrm{p}}(r) = kr\,\dot{\theta}_i \sin\theta\, dr$. The force generated by *a pair* of moving legs on opposite sides is twice that obtained by integrating along a single leg from its base at $r = R$ to its tip at $r = R + L$: $f_{\mathrm{p}} = k([L+R]^2 - R^2)\dot{\theta}\sin\theta$, and for n pairs of legs, the total propulsive force, F_{p}, at any instant is $F_{\mathrm{p}} = k\sum L_i(L_i + 2R)\dot{\theta}_i \sin\theta_i$. The drag force on a fixed leg propelled through the water with a velocity, V, depends on the angle of the leg with respect to the flow, being maximal when the leg is extended at right angles to it and around half that when it is more 'streamlined' parallel to the flow. Specifically, drag obeys the relation $f_{\mathrm{D}} = 0.5\,k\,L(1 + \sin^2\theta)V$ [21]. The drag on a pair is twice this. Batchelor shows that $k = 4\pi\eta/\ln(2/\varepsilon)$, where η is the dynamic viscosity and ε is the ratio of the thin cylindrical leg diameter to its length [21]. Added to the drag on the legs is that on the spherical body in Stokes flow, which is well known to be $6\pi\eta RV = 1.5\,kRV\,\ln(2/\varepsilon)$. Thus, the total drag force is $F_{\mathrm{D}} = kV\{1.5\,kR\,\ln(2/\varepsilon) + \sum L_i(1 + \sin^2\theta_i)\}$. Equating F_P to F_D and solving for V yields [19]

$$V = \frac{\sum_{i=1}^{n} L_i(L_i + 2R)\dot{\theta}_i \sin\theta_i}{1.5R\ln(2/\varepsilon) + \sum_{i=1}^{n} L_i(1 + \sin^2\theta_i)}.$$

Viscosity does not appear in the equation. It might seem that a higher viscosity of fluid should affect the locomotion, and indeed, a swimmer in a more viscous fluid would require more muscle power to move the legs in the same manner as in a less viscous fluid. At low *Re*, however, if two swimmers have sufficient power to generate the same leg movements in two fluids with different viscosities, they will generate the same motion and displace the same distance. It also might seem that any change in swimming velocity should depend on the velocity of the body at that instant or at an earlier time. This would be the case for swimmers with inertia, which accelerate or decelerate depending on the net momentum exerted by the moving legs on the surrounding fluid. However, a swimmer operating at low *Re* exerts no net force. Any movement of the legs simply displaces the fluid with an instantaneous response. The swimming velocity depends only on the velocity of the moving legs at that instant. As soon as the legs stop moving, the swimmer comes to a halt immediately [3].

While the appendages were assumed not to interact with each other in the model, they can approach each other and essentially behave as a single bundle. While the bundle would have a different cross section from a single appendage, the effects on the displacement are small for slender appendages [21,22]. In particular, for much of the duration of the return strokes, the appendages lie side by side and move together as such a bundle, with inter-appendage angle less than 20° (see below). To partly account for this in our model, any distinct appendages within this angular separation were replaced by a single appendage with the angles averaged. The model predictions did not depend sensitively on this threshold angle. For example, return-stroke displacements differed by typically less than 20% of an already small movement for a 10° change in threshold. In addition, appendages are feathered during return strokes, based on the observation that each appendage can be divided into two parts: a proximal set of segments and a distal set of setae. During the power stroke, the setae are extended, and the effective length of the appendage is that of the proximal segments plus the setae. During the return stroke, the setae fold posteriorly, and the effective length of the appendage in the model is reduced to the length of the proximal segments. As a further simplification for the model, all appendages were given equal lengths, set by averaging measured lengths for the three appendages during the power stroke (L_{p}, proximal segments plus distal setae) and the return stroke (L_{r}, proximal segments only). The setae are essentially removed completely during return strokes and reintroduced during power strokes. These approximations simplify the analysis without much compromise in the predictive power of the model, because the appendages are of similar length and the drag of trailing setae is much less than for extended ones. Note that all input parameters in the model are based on independent experimental measurements (table 1). The model outputs the instantaneous velocity V and thus the displacement over time of a copepod nauplius with prescribed appendage kinematics.

3. Results

3.1. Naupliar swim behaviour

The naupliar swim is characterized by a series of jerky movements that are produced by the alternation between power and return strokes of the swimming appendages. Angular positions of the first antenna (A1), second antenna (A2) and mandible (Md), measured at 0.2 ms intervals for six swim episodes, generated the input for the model for nauplii, stages 1–5 (NI–NV, table 1). Figure 2 shows the angular positions of the appendages of an NIII for 1.5 stroke cycles starting with the power stroke of the Md (triangles). Power strokes by the appendages followed a metachronal wave from the most posterior to the most anterior pair: Md followed by A2 followed by A1 (figure 2). The numbered vertical lines in figure 2 indicate the time for the minimum (1), maximum (3) and median (2 and 4) angular positions of the A1, and the corresponding video images of the swimming nauplius are shown below. Just prior to the return stroke, all three appendages are at their maximum angular position, and they appear to bend with the distal setae pointing posteriorly in preparation for 'feathering' (figure 2*c*; '3'). The return strokes of the three appendages started approximately at the same time (figure 2*b*, '3') with the A1 and the A2 moving together for much of the duration. The return stroke of the Md was shorter and reached its minimum angle first. The A2 completed the return stroke next and the A1 last. The Md was also the first appendage to initiate the subsequent power stroke ($T = 14.2$ and 23.6 ms), and its angular excursion was half completed by the time the A1 initiated its power stroke (figure 2, '1'). The nauplii of all stages completed the power and return

Table 1. Morphological parameters of nauplii.

		body size (μm)		proximal unit (μm)			seta length (μm)		
nauplius	stage	length	width	A1	A2	Md	A1	A2	Md
N172	NI	71	44	37	40	26	26	22	21
N182	NII	78	46	35	34	33	32	20	20
N178	NIII	97	47	35	33	24	25	30	23
N189	NIV	124	54	38	38	32	25	26	20
N201	NV	145	64	42	43	34	27	38	22
N207	NV	149	76	41	31	35	27	35	26

strokes in approximately 10 ms during the rapid swim, which corresponded to a beat frequency of 100 Hz (range 85–135 Hz; $n = 11$).

The temporal progression of appendage movements in the coordinated patterns can be represented graphically as bars placed along a time axis, depicting the duration of each state for each appendage over successive swim cycles (figure 3). The relationships between power strokes (solid bars), recovery strokes (hatched bars) and stationary periods (clear bars) for each appendage pair are shown for either two (five top traces) or four (bottom trace) complete cycles (figure 3). Each swim episode was initiated with a synchronous power stroke of the three pairs of appendages. This was followed by an immediate change in gait: subsequent power strokes were produced by a metachronal wave (the pattern of diagonally ascending solid bars). In most cases, appendage pairs transitioned through brief stationary periods between the power and the return stroke, and vice versa. These stationary periods were offset from each other, so that in nearly all cases at least one pair of appendages was always moving. During the power strokes, only pairs of adjacent appendages (A1 and A2, or A2 and Md) overlapped (N201 being an exception), whereas in nearly every return stroke, all three pairs of appendages overlapped during some portion of the recovery period. The transition from power to return stroke included a period when pairs of appendages moved in opposite phases, specifically the return stroke of the Md (hatched bar) was almost always initiated before the completion of the A1 power stroke (solid bar). However, comparisons among the plots also showed that the details of the timing of power, return and stationary phases varied among swim episodes, and even between cycles within a single swim episode.

Phase relations and their progression during a swim cycle can be seen more clearly by plotting angles of two pairs of appendages against each other, generating a Lissajous curve of the cyclical activity (figure 4*a*). The lines between points show the progression of the paired angles over time as the appendages move during the power and return strokes (arrows). The synchronous movement of three pairs of appendages during the return stroke is clearly visible by the A1–A2 (left) and Md–A2 (right) trajectories nearly superimposing on the 45° line (dashed line). In contrast, during the power strokes, the trajectory for each appendage pair describes a sweeping arc representing the changing phase states of the metachronal coordination pattern (figure 4*a*). In the model, the three pairs of appendages are treated as a single unit if their respective angles are within 20° of each other as indicated by the trajectories inside the dotted lines (figure 4*a*).

The three pairs of appendages differed both by their relative position with respect to the body axis, and by their angular excursion. In the example shown in figure 2, the A1 completed an arc of *ca* 120° centred around 70°, whereas the Md excursion was less than 60° and centred at 135°. The angular excursion of the A2 was intermediate at 100° and centred around 90°. The antennae, A1 and A2, typically had angular excursions of at least 100°, often exceeding 130°. Maximum excursions of the Md were near 90°, although in three swim episodes we observed excursions that were closer to 60° (table 2). The relative placement of the appendages to each other is a function of the articulation of the appendage and its minimum and maximum angles during the swim cycle. This relationship was computed for each swim episode as the angular separation between the mid-excursion angle for each pair of appendages varied between 20° and 40° as shown in figure 4*b*.

The translation of power and return strokes of the individual appendages into naupliar displacement is shown in figure 5. In general, forward motion corresponded to the power strokes of the appendages (time periods: 0–4, 9–15 and 20–25 ms), whereas backward motion occurred during return strokes (time periods: 6–7.5, 16–18 ms). The displacement during the first cycle, which is produced by synchronous power strokes of the appendages, is shorter than the displacements of subsequent cycles with a metachronal sequence of power strokes (see also figure 3). The initial forward displacement averaged 0.6 body lengths, whereas the displacements produced by the second and third power strokes averaged 1 and 0.8 body lengths, respectively ($n = 11$). The backward displacements produced by the return strokes were similar across cycles and averaged between 0.16 and 0.20 body lengths. For the second and third cycles, these backward displacements represented a 20% backwards slide compared with the preceding forward gain ($n = 11$). This pattern was observed in all naupliar developmental stages.

Additional patterns emerge when the relationship between displacement and appendage movement is analysed in more detail. For each swim episode, the phase diagram in figure 3 shows the timing of forward (right pointing arrows) and backward (left pointing arrows) displacement, each separated by a brief stationary phase (grey). Between the backward and forward displacements, this period was relatively long and corresponded to a time when the Md and the A1 were in opposing phases (figure 3, grey between arrow heads). After the forward displacement, the stationary period was typically very short and often occurred during the return stroke of one or more pairs of appendages (figure 3, grey between arrow

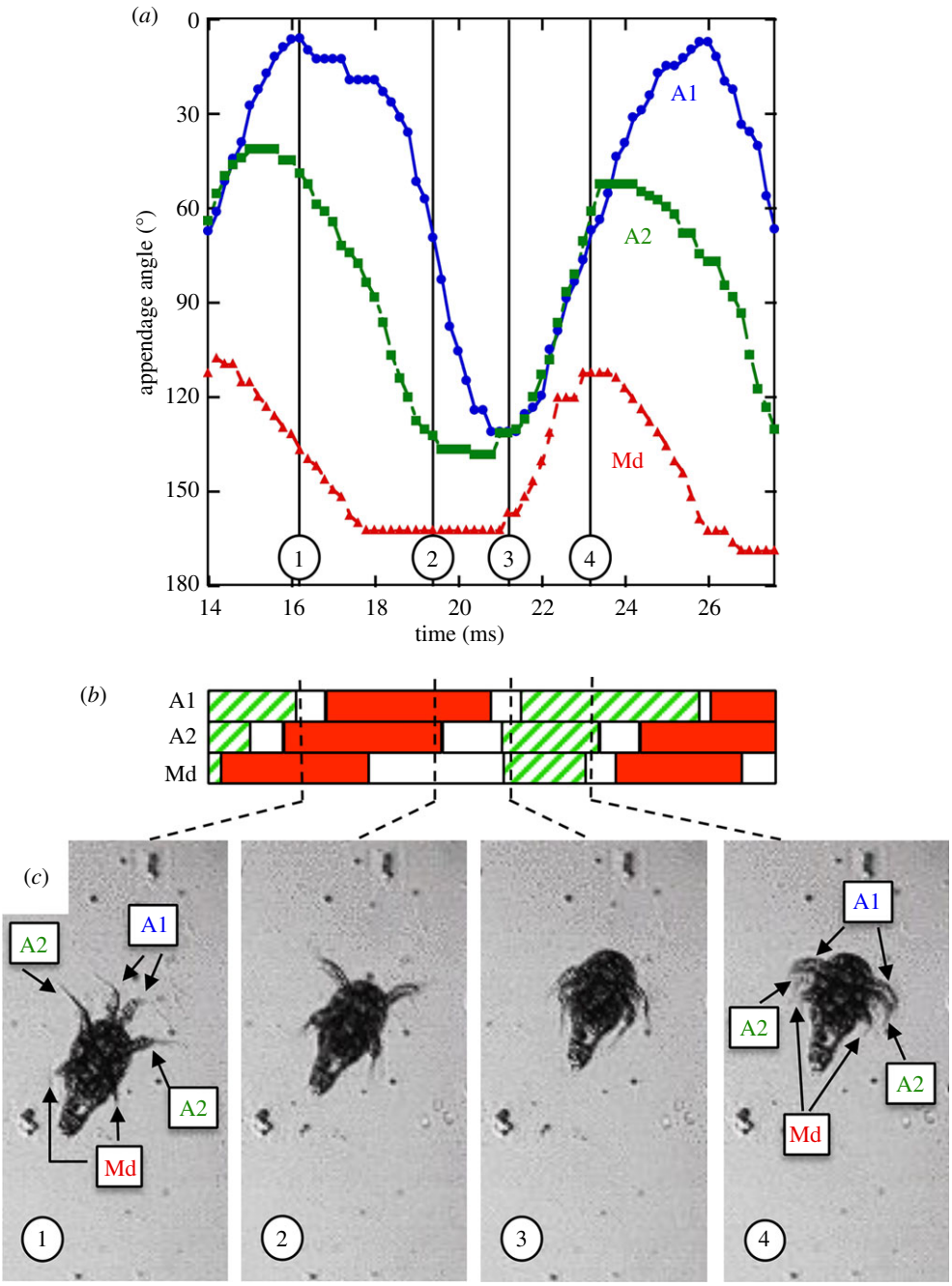

Figure 2. Appendage angles and timing of power and return strokes during 1.5 cycles of swim sequence in a stage 5 nauplius (NV, N201). (*a*) Appendage angle with respect to body axis during power and return strokes. The sequence starts at the beginning of the third cycle (14 ms) with the power stroke of the Md and ends after the completion of the following power stroke ($T = 28$ ms). Circles: angular position of A1 (blue); squares: angular position of A2 (green); and triangles: angular position of Md (red). Temporal resolution: 0.2 ms. Numbers 1–4 correspond to each video image, and represent minimum (1), maximum (3) and mid-point (2, 4) angular positions of the A1. (*b*) Temporal progression of power and return strokes and stationary periods for A1, A2 and Md. Solid bars: power stroke (Pwr, red); hatched bars: return stroke (Rtn, green); open bars: stationary phase (Sta, white). Vertical dashed lines correspond to images 1–4. (*c*) Video images taken at the indicated times (1–4) showing the relative position of the nauplius and its appendages (A1, A2 and Md). (Online version in colour.)

tails). Furthermore, forward displacements were longer than backward ones, and this difference was disproportionate to the relative duration of power and return strokes by the appendages (figure 3, right versus left arrows).

3.2. Comparison between experimental and model-predicted locomotion

3.2.1. Amplitude of appendage excursions

The model was run using morphological and angular data obtained from each of the six naupliar swim episodes (tables 1 and 2). Figure 6 shows experimental data and model output for a four-cycle swim episode of a stage 5 nauplius (NV; N201), with the angular measurements used as model input shown in figure 6*a*. This episode offers a good dataset to test the model, because displacements per cycle were small initially, so inertia was small as assumed in the model. In addition, this nauplius varied the stroke amplitudes over time and produced non-periodic cycles, which can be readily inputted into our model. Appendage excursions for this nauplius increased over the first three cycles as shown in figure 6*a*. In particular, the angular excursion of the first antenna (A1) nearly quadrupled between the first and third cycles. The experimentally measured displacements (figure 6*b*, black line) are superimposed on the predicted displacements (grey line). The model output

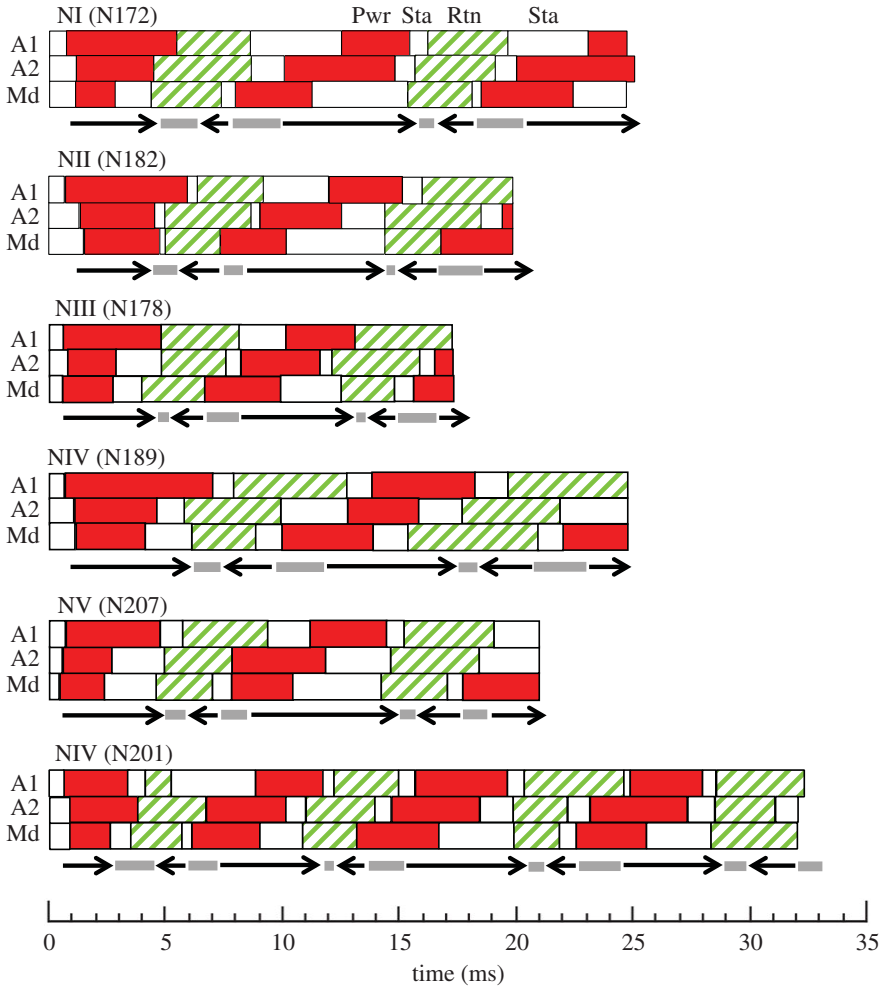

Figure 3. Timing of power and return strokes of appendages and displacement of the body in six rapid swim episodes for *Bestiolina similis* nauplii from different stages (NI, N172; NII, N182; NIII, N178; NIV, N189; NV, N207 and N201). All swim episodes start with the nauplius at rest. Solid bars: power stroke (Pwr, red); hatched bars: return stroke (Rtn, green); open bars: stationary phase (Sta, white). The timings of forward and backward displacements are shown below each set of bar graphs as black arrows (right arrow, forward; left arrow, backward), with grey lines showing the periods of no movement (stationary) in between each power and return stroke. (Online version in colour.)

successfully predicts the forward, stationary, backward and second stationary phases of the locomotory pattern. The model is in good agreement with respect to observed timing and the distances moved, particularly for the first 20 ms, validating its basic approximations. The displacement per cycle, both observed and simulated, increases progressively with time, which is attributable to the increasing amplitude of the A1, suggesting, not surprisingly, that the amplitude of an appendage excursion alone can have a significant effect on the displacement of the nauplius. The model predicts velocity directly, with displacement of the body reflecting the integration of this velocity over time (figure 6*b*). Unfiltered plots of velocity *per se* are too noisy to be useful owing to the high frame rate and pixel resolution of the images. Smoothing velocity with a five-point running unweighted average provides a less noisy result, as shown in figure 6*c*. Velocity peaks by and large agree between predicted and observed in both time and magnitude, both power and return strokes (first return stroke being an exception). *Re* peaks around 2 for the first two cycles, rising above 3 for the last two (right side ordinate).

3.2.2. Inertial effects

A closer comparison between model output and observed displacement showed that discrepancies in magnitude as well as timing of displacement increased over time (figure 6*b*). The observed velocities also tend to lag behind those predicted (figure 6*c*). In particular for the final cycle tracked in the swim trajectory shown in figure 6, predicted backward movement commenced earlier than that observed, and was of greater magnitude. The subsequent forward movement predicted was very close to that observed, but again, the following backward movement commenced earlier and was of greater magnitude. The model underestimated the forward displacement to the end of the fourth return stroke by 11%. This discrepancy is attributed to increasing effects of inertia as distance moved and peak velocities increased with swim cycle. The velocity lag is also what would be expected from inertial effects. This is further illustrated in figure 7*a*, showing plots of both the predicted and observed peak forward and backward displacements and their timing in each of the first two swim cycles in the six nauplii (including N201), along with their mean values and standard deviations. The timing discrepancies in local maxima/minima average 0.6 ms, and they are significant at the $p < 0.005$ level (one-tailed; sign test). Plotting the predicted forward or backward displacements against those actually observed showed an increasing discrepancy between prediction and observation with larger forward displacements (figure 7*b*). These results suggest that inertial effects are a likely explanation for the differences between model and observed displacements.

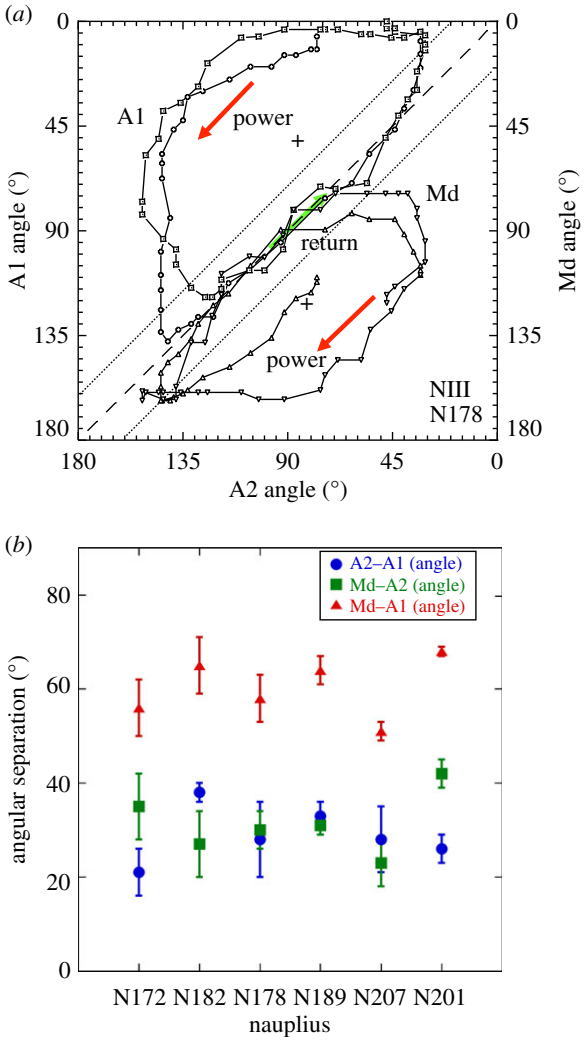

Figure 4. (*a*) Lissajous curves generated by plotting the angular positions of adjacent appendages against each other as they evolve over two swim cycles (A1–A2 above, and A2–Md below the 45° line; dashed line). Each point represents angular positions at 0.2 ms intervals for the swim trajectory of a nauplius stage 3 (NIII, N178). Power and return strokes are indicated by arrows with the return stroke along the 45° line (diagonal down arrows: power (red); diagonal up arrow: return (green)). The dotted lines (20° above and below the 45° line) indicate the range that the model considers two or three appendages as a single entity when computing drag. Crosses indicate average separation between pairs of adjacent appendages. (*b*) Angular separation and standard deviations between two appendages at the mid-point of their excursions computed for the second and third stroke cycles for excursions for swims in different developmental stages. Circles, A2–A1 (blue); squares, Md–A2 (green); and triangles, Md–A1 (red). Nauplius developmental stage: N172, NI; N182, NII; N178, NIII (shown in *a*); N189, NIV; N207, NV; N201, NV. (Online version in colour.)

3.3. Testing paddling parameters using the model

Given a model that does not require any fitting of parameters and the good agreement between model and observation for the N201 swim episode, we used it to study the effect of alternative forms of appendage actuation on displacement.

3.3.1. Paddle asymmetry—folding setae

To assess the importance of seta folding on net displacement, the phase differences among the three pairs of appendages were eliminated from the model while leaving setal folding intact, as shown in figure 6*a* (dashed lines). This was effected by delaying the timing of the A2 and Md strokes by 1 and 2 ms, respectively, so that all appendages moved in synchrony. The resulting predicted displacement was significantly smaller than both the observed displacement and that predicted by the full model with both factors active. Thus, the 36% reduction (to 70 from 110 μm) in the effective appendage lengths during the return stroke produces a predicted displacement that is 55% of that of the full model, as shown in figure 8*a* (middle trajectory).

3.3.2. Phase lag

To assess the importance of phasing of appendage movements, the appendages were all allowed to retain their original length equal to the combined length of the proximal segments and the setae. The setae were not folded at any time during the cycle, so that each appendage had the same resistance moving forward as moving back. In this case, the nauplius was still predicted to move forward because of the phase lag between adjacent appendages during the power stroke [19], and the transition to effectively a single appendage during the synchronous return stroke, but the predicted displacement was again much smaller than that of the full model (as well as of the experimental data) representing 21% of the originally predicted displacement (figure 8*a*). Further, the sum of net displacements from setal folding and phase lag separately is less than the displacement produced by combining the two factors, indicating that the effects are nonlinear and reinforce each other (figure 8*a*). Thus, the commonly recognized propulsive mechanism of appendage feathering is enhanced by an adjustment of phase relations.

3.3.3. Selective removal of paddles

We used the model to study the relative contribution of each of the three pairs of appendages to displacement. Figure 8*b* shows the model predictions for the displacement when one of the pairs of appendages is removed. In each case, the predicted net displacement was smaller than before. The difference was particularly significant with the absence of either the A1 or the A2, indicating that they were both crucial for the forward movement during the power stroke. In the absence of the mandible, the forward movement was unaffected; however, the backward movement was greater than the observed, leading to a smaller net displacement (figure 8*b*). Thus, each appendage contributed to net displacement of the nauplius, but the nature of the contribution differed among appendages.

Although removal of two pairs of appendages reduced theoretical net displacements significantly, net forward displacements were still predicted, owing to setal folding, even when the Md was the only appendage (figure 8*c*). The A2 produced the greatest net displacement by itself (figure 8*c*), which is not surprising given that the mid-point of its angular excursion is the closest to a right angle, thus providing the greatest displacement for any given amplitude of angular excursion.

3.3.4. Stroke amplitude and spacing between appendages

The model was used in a study of optimization of net displacement. Based on the swim episodes that were analysed, we established an 'idealized' pattern for the timing of the appendage movements as input for the model. We suppose that all three appendages oscillate with constant amplitude at constant angular speed, and the mid-point angles of adjacent appendages are a constant angle apart. The phases of the strokes are adjusted, so that the appendages return together. During that time, they are merged into a single appendage (figure 9*a*, bar above plot).

Table 2. Kinematic parameters.

	appendage mid-angle (°)[a]			angular excursion (°)[b]				
nauplius	A1	A2	Md	A1	A2	Md	frequency (Hz)	no. of cycles
N172	70	91	126	130	125	88	93	2
N182	55	93	120	107	110	68	102	2
N178	64	92	122	125	118	83	119	2
N189	62	94	125	102	90	64	89	2
N201	60	96	139	86	90	51	122	4
N201[c]	75	98	138	128	92	56	111	2
N207	72	100	120	134	130	86	122	2

[a]Mid-point angles (angular position half-way between extremes) excluded angles for the initial rest position.
[b]Maximum angular excursions for the different naupliar appendages during swimming bouts excluding the first angular excursion from rest to the end of the first power stroke. Numbers of cycles indicated in last column.
[c]Averages are for cycles 3 and 4.

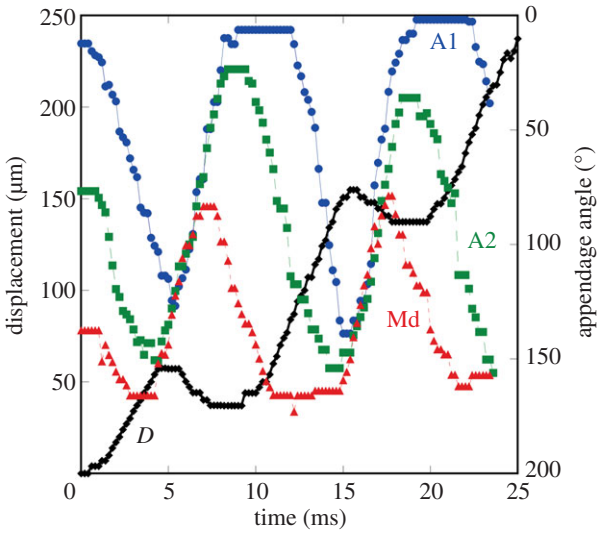

Figure 5. *Bestiolina similis* naupliar displacement (*D*: diamonds, black) and angular excursion of three sets of appendages during 2.5 swim stroke cycles measured at 0.2 ms intervals for a nauplius stage 1 (NI, N172) swim episode. Nauplius was stationary at the beginning of swim episode ($T = 0$ ms), displacement in micrometres over time from initial location ($D = 0$). Circles, angular position of A1 (blue); squares, angular position of A2 (green); and triangles, angular position of Md (red). (Online version in colour.)

This 'idealized' pattern produces the key observed behavioural components of metachronal power strokes starting with the Md and ending with the A1, as well as maintaining partial synchrony during the return strokes.

The model was tested for a combination of angular spacing (φ) between adjacent appendages between 0° and 45° and amplitude (α) of the appendage excursion from the mid-point to either maximum or minimum angular position from 0° to 90°, as diagrammed in figure 9*a*. For this analysis, the model incorporated three simplifications: (i) folding of setae was omitted, (ii) spherical body was replaced by a point, and (iii) appendages with identical angles were bundled together during the return strokes. Results are shown in figure 9*b* as a 'heat map' with warmer colours indicating larger net forward displacements (see figure caption for details), which are attained in the approximate ranges of $40° < \alpha < 70°$ and $20° < \varphi < 30°$.

Interestingly, the experimental data for several nauplii are within or close to these ranges (figure 9*b*). The theory predicts that displacements remain large over wide ranges of α and φ close to the optimum. The model suggests that, by exhibiting a swimming behaviour close to the theoretical optimum, nauplii can afford to vary the appendage excursions over time and across different episodes (as observed) without much compromise in displacement. However, the current analysis does not incorporate setal feathering or drag on the body; the computed displacements are only indicative of the maximum possible displacement per cycle.

4. Discussion

Organisms, including nauplii, depend on locomotion to search for and capture food, relocate in space and escape from potential predators. Copepods are the preferred prey of many different planktivores, and all developmental stages (nauplii and copepodites) are under selection for effectively avoiding predators. Effective locomotion under the low *Re* regimes that render their aquatic habitat 'sticky' for motion is clearly of key value. The model analysis here has extended our understanding of how the naupliar body plan in combination with a coordinated beat pattern of three pairs of appendages achieve that locomotion.

The smaller an organism, the more dominant viscous forces are expected to be in comparison with inertial forces at any given swimming speed. Nauplii of copepod species like *B. similis* are among the smallest free-living metazoans [23], and thus are among the smallest aquatic organisms that depend on paddles for locomotion. Because of their size, they should be among the better organisms for models limited to low *Re* regimes. Thus, we have been able to simulate locomotion by accounting just for the viscous forces and ignoring the inertial ones. The model is dependent only on measured morphological parameters and kinematic data. Discrepancies between model and observation have given more insights into the kinematics of the swim, including the role each appendage-paddle plays in locomotion, the effect of feathering compared with the effect of return-stroke synchrony on net displacement, and when inertial forces might contribute to locomotion.

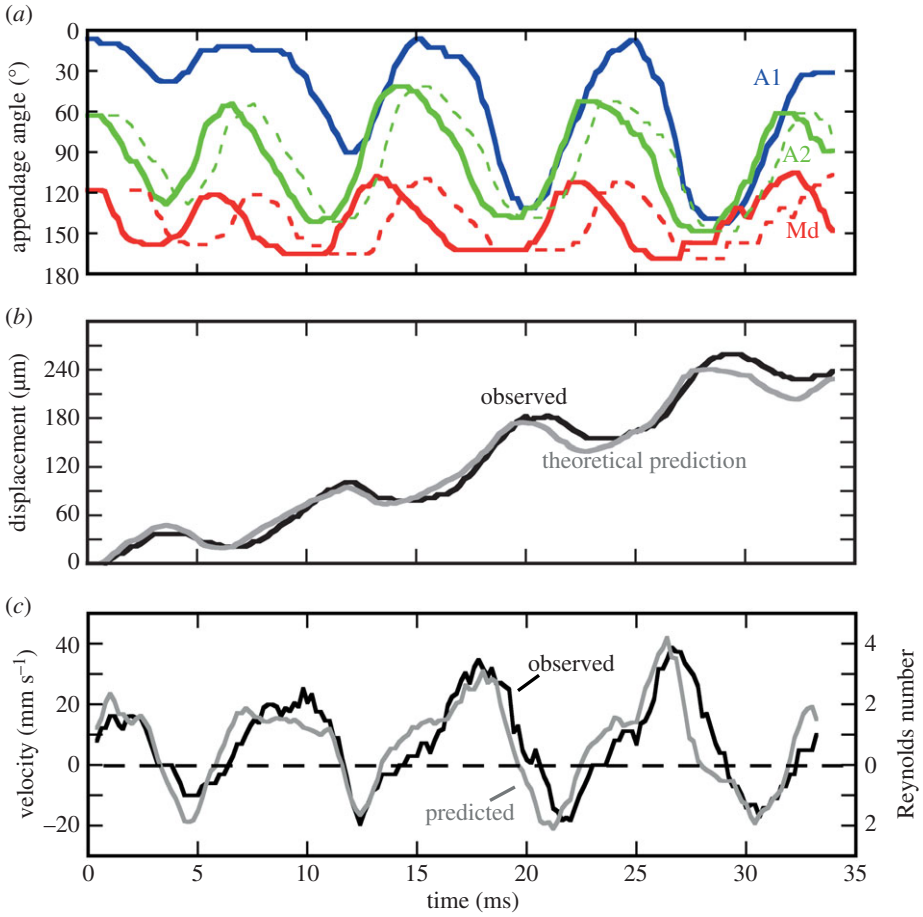

Figure 6. Model input (*a*) and model prediction of naupliar displacement (*b*) and velocity (*c*). (*a*) Solid lines show angular position of three appendages at 0.2 ms intervals starting from rest ($T = 0$ ms) to completion of fourth return stroke ($T = 32$ ms) from an observed swim episode (NV, N201). Solid lines represent measured angles of appendages as labelled. Top line: A1 (blue); middle line: A2 (green); and bottom line: Md (red). Dashed lines show angular position of the A2 and Md displaced temporally 1 and 2 ms, respectively, to be in phase with the A1. Top dashed line, A2 (green); bottom dashed line, Md (red). These modified angular position curves were used as model input to study the effect of phase on displacement (figure 8*a*). (*b*) Copepod displacement over time: observed (black line) and theoretical model prediction (grey). (*c*) Copepod velocity over time: observed (black line) and theoretical model prediction (grey). Five-point (1 ms) moving averages. Reynolds numbers along right scale calculated using mean diameter of nauplius.

This model extends two previous models of swimming in crustacean nauplii. One was developed by Williams [5,6] to simulate naupliar and metanaupliar kinematics in *Artemia*, whereas the second one was used to examine the effect of viscosity and temperature regimes on the swimming behaviour of copepod (*Acartia tonsa*) nauplii [14]. In these earlier models, the nauplius swims by imparting momentum on the surrounding water, a fundamentally different mechanism of propulsion from our model in which the nauplius swims by rearranging the water without exerting any net force. The earlier models make assumptions about the coefficient of drag and other parameters in the absence of direct measurements, whereas ours is based completely on direct measurements. Furthermore, in accordance with usage patterns observed in their species, Williams [7] and Gemmell *et al*. [14] simulated only one (A2) or two (A1 and A2) pairs of appendages, respectively. We simulated all three pairs, in accord with our own observations on *Bestiolina*, and this is the more usual pattern observed in copepod nauplii [10,24]. The *Acartia* model was limited to full-sweep (180°) appendage excursions, in order to investigate maximum performance [14]. However, 0–180° is an extreme range that we have not observed in the fast swims of *B. similis* nauplii here, so our studies used measured appendage movements with smaller excursions (cf. figure 9). Gemmell *et al*. [14] varied the duration of the power phase relative to that of the return phase in the model, and concluded that this variation alone is responsible for the changes in displacement of nauplii swimming in fluids with different viscosities and temperatures. In our model, stroke duration has no effect on net displacement, nor does viscosity enter into the mathematical equation predicting low *Re* swimming. Thus, the dependences observed in the *Acartia* model would be an indication of locomotion in a higher *Re* regime than what we have modelled. In contrast, we investigated the effect of other factors, such as appendage number, amplitude and phase, on locomotion.

Crustacean nauplii differ in appendage morphology, kinematics and the number of appendages used for locomotion [5,18,24,25]. Based on earlier observations of swimming in nauplii and model simulations, these differences lead to functional plasticity in locomotion [5]. The current modelling studies confirm and extend the conclusion that the nauplius bodyplan allows for flexibility in swimming. The model provides quantitative data on how locomotion changes as a function of the amplitude of the stroke excursion, and its relative angular orientation with respect to the direction of movement. Unlike organisms with paddles distributed along an elongate body [13,15], the A1 and Md are constrained to non-optimal angles because of a compact spheroidal body. Thus, the model predicts (figure 8) that the greatest displacement is generated by the middle pair of appendages, the A2, whose sweep is centred optimally for forward thrust, near 90°. Not surprisingly,

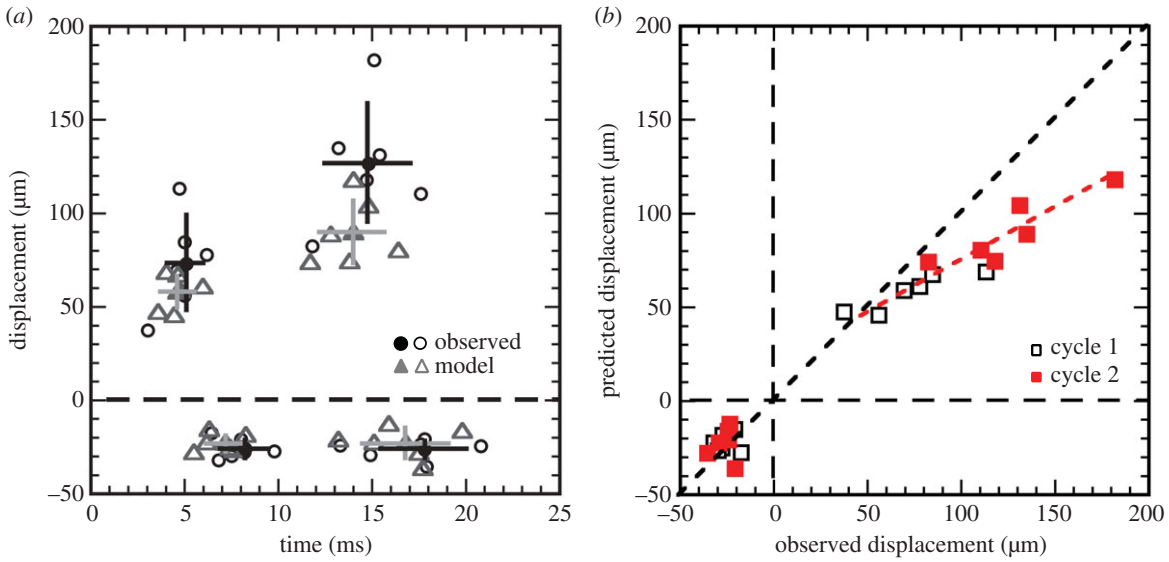

Figure 7. Comparison between model predictions and experimental observations. (*a*) Observed (circles, black) and predicted (triangles, grey) displacements in micrometres for first and second power (positive values) and return (negative values) strokes for individual swim episodes (open symbols) and means and standard deviations (solid symbols and lines). (*b*) Relationship between observed and predicted displacements for forward and backward movements during the first (open squares) and second (solid squares, red) swim cycles. (Online version in colour.)

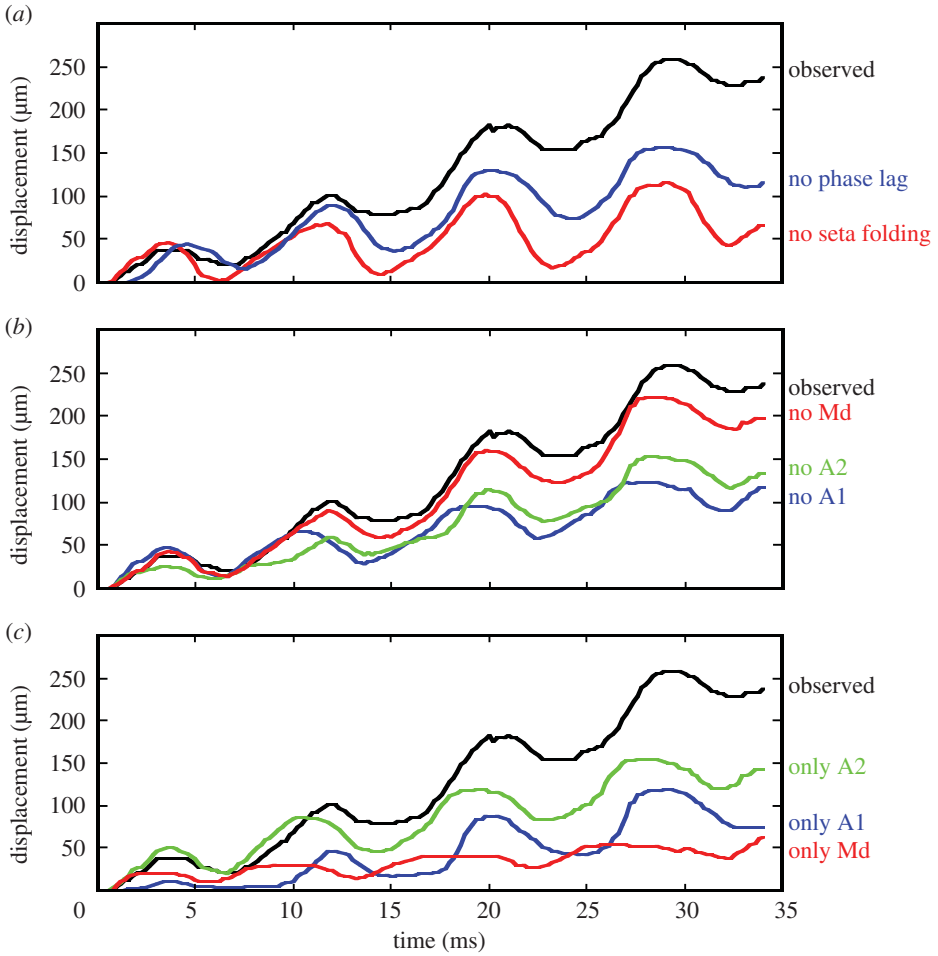

Figure 8. Model tests show predictions of naupliar displacement using different input parameters as labelled. (*a*) Effect of folding of setae (= shortening length of appendages) during the return stroke on predicted displacement (bottom line, red) and effect of removing the phase lag between appendages (middle line, blue; see figure 6*a* dashed lines for model input) on predicted naupliar displacement; and observed data (top line, black). (*b*) Effect of removal of one appendage on predicted naupliar displacement: removal of first antenna (no A1; bottom line, blue), removal of second antenna (no A2; second line from the bottom, green); removal of mandible (no Md; third line from the bottom, red); and observed data (top line, black). (*c*) Effect of removal of two appendages on predicted naupliar displacement: only mandible (only Md; bottom line, red); only first antenna (only A1; second line from bottom, blue); only second antenna (only A2; third line from bottom, green); and observed data (top line, black).

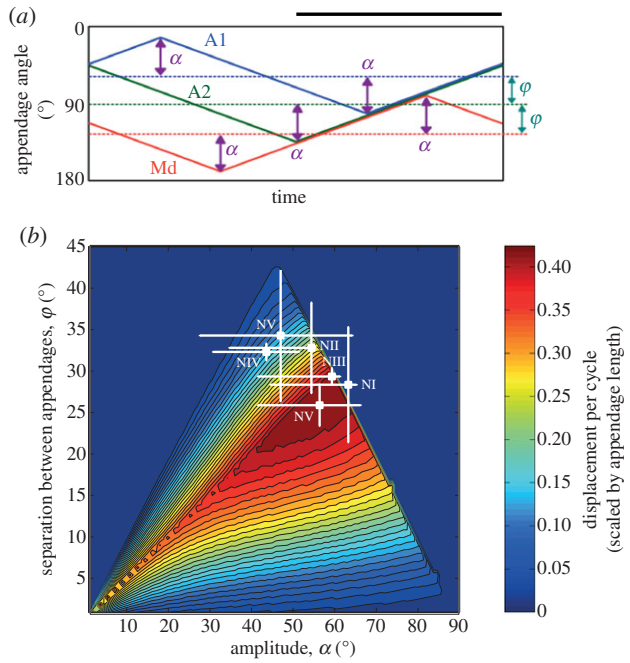

Figure 9. Effect of stroke amplitude and separation between appendages on predicted net displacement. (*a*) Idealized angular excursion of appendages used to study the effect of changing φ (angular separation between appendages at the mid-point of their excursion) and changing α (the amplitude of the excursion of the appendages on either side of the mid-point angle). The model set the body radius (R) to zero, and during return strokes, omitted folding of setae, but merged appendages with coincident angles into a single appendage. (*b*) Model output predicting the net forward displacement per cycle for given (α, φ) pairs, presented as a 'heat map'. The displacement increases from the edges toward the centre of the map as the shade changes from blue to red. Crosses labelled with naupliar stage represent observed data from *Bestiolina similis* nauplii. The model was only run for cases in which there is overlap of all three appendages for at least a part of the return strokes (i.e. $\alpha > \varphi$). Also omitted were points in the range $\alpha + \varphi > 90^\circ$ in which the appendage angles went outside of the acceptable range of $0-180^\circ$. A ridge of locally high displacements follows the line $\varphi = \alpha/2$, falling off steeply for lines with greater slope and less steeply along those with lesser slopes. A1, first antenna; A2, second antenna; Md, mandible. Time period when two or more appendages move together is indicated by bar above graph (*a*).

all crustacean nauplii use the A2 for swimming, and sometimes this is the only appendage used for locomotion, as in the brine shrimp (*Artemia franciscana*) [6,10].

The model predicts lower net displacements when either the A1 or the Md is not involved in swimming (figure 8*b*). Some crustacean nauplii use primarily two pairs of appendages. The cirripeds swim using the A2 and Md (*Balanus* sp., *Lepas pectinata*) [10,26], whereas the copepod *A. tonsa* swims with the A1 and A2 [24]. Specifically, when the Md is excluded, forward displacement is unchanged, whereas the backward slide during the return stroke is greater (40% versus 20% of forward displacement). Experimental data for *A. tonsa* indicate a backward displacement of approximately 33% of forward movement, which is greater than that observed in copepod nauplii using three pairs of appendages (approx. 20%; this study, [24]), which is consistent with model results (approx. 22%, second cycle, figure 7*a*). Thus, one key component of the kinematics of the copepod nauplius' fast swim is the use of two pairs of appendages to optimize forward propulsion, and the third (mandible) to minimize backward movement during return strokes.

The naupliar swim is characterized by rapidly changing velocities (this study) [25]. Thus, nauplii inhabit a physical environment where the relative contributions of viscous and inertial forces are continuously changing through each swim cycle. For an organism of a particular size, inertial forces become more important as velocity increases. The model provides some insights into this—an examination of the discrepancy between the predicted forward versus backward displacements suggests better agreement for the smaller backward movement, which would be expected given that inertial forces are not factored into the model. This is further supported by the experimental observation that the duration of the forward progression extends beyond the completion of the appendage power strokes even in the smallest nauplii. Furthermore, between the power and return strokes the stationary phase in body movement occurs after the return stroke has already been initiated in all three pairs of appendages. Both these observations are consistent with the fact that the nauplius is coasting after completing the power stroke. Using particle-tracking velocimetry, Wadhwa *et al*. [27] observed that a pair of vortices was generated by a swimming nauplius and that these persisted well after the swim episode had terminated, suggesting that inertial forces are not negligible. This would be particularly true for larger nauplii ($L = 170-260$ µm) swimming at $Re > 7$ as calculated by Wadhwa *et al*. [27]. Even in the case of *B. similis* nauplii, especially for the longer displacements in any one power stroke, the peak displacement was reached significantly after that predicted by the model based on observed appendage movement, which suggests the animals were carried forward by momentum (figure 7*a*). Thus, the effectiveness of the escape swim may hinge on the nauplius' ability to exploit inertial forces, and may even place a minimum size limit on these planktonic nauplii. The model will need to be refined to include both viscous and inertial forces to be more broadly applicable, in order to enable a better understanding of how viscous and inertial forces interact during naupliar locomotion.

5. Conclusion

Naupliar displacement over time was computed using a model based on slender-body theory for Stokes flow. The model only depended on morphological measurements and empirically determined kinematics of three pairs of appendages. Net forward displacement in the nauplius is increased by the combination of setal folding and phase lag of the power strokes with synchronous return strokes. The model's quantitative analysis demonstrated that these two effects are nonlinear, and net displacement is greater than the sum of the two factors acting individually. For swim cycles with small displacements, the model accurately simulated locomotion taking only viscous forces into consideration. However, discrepancies between model predictions and observations increased with the magnitude of forward displacements. These results suggest that inertial forces can contribute to locomotion even in the smallest nauplii. The interaction between viscous and inertial forces is highly dynamic during a swim cycle characterized by continuously changing velocities.

Ethics. Institutional guidelines for research on invertebrates were followed.

Data accessibility. Data summaries on experimental results are available through the Biological & Chemical Oceanography Data Management Office (http://www.bco-dmo.org/project/562097).

Authors' contributions. P.H.L., D.T. and D.K.H. conceived of, designed and coordinated the study, drafted the manuscript and gave final approval for publication. P.H.L. and D.K.H. acquired the experimental data, and completed data analysis. D.T. developed and tested the model.

Competing interests. We declare we have no competing interests.

Funding. This study was partially supported by the National Science Foundation (grant nos. OCE 12-35549 and OCE 04-51376 to P.H.L. and D.K.H.) and the College of Natural Sciences, U. Hawaii at Manoa (D.T.).

Acknowledgements. We thank Kyle VanderLugt for providing the copepod nauplii, Angel Yanagihara for access to the high-speed video camera, Jenn Kong for the nauplius scanning electron micrograph and Stanford Togashi for assisting with video data processing.

References

1. Lauga E, Powers TR. 2009 The hydrodynamics of swimming microorganisms. *Rep. Prog. Phys*. **72**, 096601. (doi:10.1088/0034-4885/72/9/096601)
2. Guasto JS, Rusconi R, Stocker R. 2012 Fluid mechanics of planktonic microorganisms. *Annu. Rev. Fluid Mech*. **44**, 373–400. (doi:10.1146/annurev-fluid-120710-101156)
3. Purcell EM. 1977 Life at low Reynolds number. *Am. J. Phys*. **45**, 3–11. (doi:10.1119/1.10903)
4. Blake RW. 1986 Hydrodynamics of swimming in the water boatman, *Cenocorixa bifida*. *Can. J. Zool*. **64**, 1606–1613. (doi:10.1139/z86-242)
5. Williams TA. 1994 The nauplius larva of crustaceans—functional diversity and the phylotypic stage. *Am. Zool*. **34**, 562–569. (doi:10.1093/icb/34.4.562)
6. Williams TA. 1994 Locomotion in developing *Artemia* larvae—mechanical analysis of antennal propulsors based on large-scale physical models. *Biol. Bull*. **187**, 156–163. (doi:10.2307/1542238)
7. Williams TA. 1994 A model of rowing propulsion and the ontogeny of locomotion in *Artemia* larvae. *Biol. Bull*. **187**, 164–173. (doi:10.2307/1542239)
8. Vogel S. 1994 *Life in moving fluids*, 2nd edn. Princeton, NJ: Princeton University Press.
9. Walker JA, Westneat MW. 2000 Mechanical performance of aquatic rowing and flying. *Proc. R. Soc. Lond. B* **267**, 1875–1881. (doi:10.1098/rspb.2000.1224)
10. Gauld DT. 1959 Swimming and feeding in crustacean larvae: the nauplius larva. *Proc. Zool. Soc. Lond*. **132**, 31–50. (doi:10.1111/j.1469-7998.1959.tb05511.x)
11. Kohlhage K, Yager J. 1994 An analysis of swimming in remipede crustaceans. *Phil. Trans. R. Soc. Lond. B* **346**, 213–221. (doi:10.1098/rstb.1994.0142)
12. Alexander RM. 2003 *Principles of animal locomotion*. Princeton, NJ: Princeton University Press.
13. Alben S, Spears K, Garth S, Murphy D, Yen J. 2010 Coordination of multiple appendages in drag-based swimming. *J. R. Soc. Interface* **7**, 1545–1557. (doi:10.1098/rsif.2010.0171)
14. Gemmell BJ, Sheng J, Buskey EJ. 2013 Compensatory escape mechanism at low Reynolds number. *Proc. Natl Acad. Sci. USA* **110**, 4661–4666. (doi:10.1073/Pnas.1212148110)
15. Zhang C, Guy RD, Mulloney B, Zhang QH, Lewis TJ. 2014 Neural mechanism of optimal limb coordination in crustacean swimming. *Proc. Natl Acad. Sci. USA* **111**, 13 840–13 845. (doi:10.1073/pnas.1323208111)
16. Mauchline J. 1998 *The biology of calanoid copepods*. *Advances in marine biology*, vol. 33 (eds JHS Blaxter, AJ Southward, PA Tyler). New York, NY: Academic Press.
17. McKinnon AD, Duggan S, Nichols PD, Rimmer MA, Semmens G, Robino B. 2003 The potential of tropical paracalanid copepods as live feeds in aquaculture. *Aquaculture* **223**, 89–106. (doi:10.1016/S0044-8486(03)00161-3)
18. Bradley CJ. 2009 *Development of copepod escape behaviors in response to a hydrodynamic stimulus*. Honolulu, HI: University of Hawaii at Manoa.
19. Takagi D. 2015 Swimming with stiff legs at low Reynolds number. *Phys. Rev. E* **92**, 023020. (doi:10.1103/PhysRevE.92.023020)
20. VanderLugt K, Lenz PH. 2008 Management of nauplius production in the paracalanid, *Bestiolina similis* (Crustacea: Copepoda): effects of stocking densities and culture dilution. *Aquaculture* **276**, 69–77. (doi:10.1016/J.Aquaculture.2008.01.041)
21. Batchelor GK. 1970 Slender-body theory for particles of arbitrary cross-section in Stokes flow. *J. Fluid Mech*. **44**, 419–440. (doi:10.1017/S002211207000191X)
22. Becker LE, Koehler SA, Stone HA. 2003 On self-propulsion of micro-machines at low Reynolds number: Purcell's three-link swimmer. *J. Fluid Mech*. **490**, 15–35. (doi:10.1017/S0022112003005184)
23. McClain CR, Boyer AG. 2009 Biodiversity and body size are linked across metazoans. *Proc. R. Soc. B* **276**, 2209–2215. (doi:10.1098/Rspb.2009.0245)
24. Borg CMA, Bruno E, Kiørboe T. 2012 The kinematics of swimming and relocation jumps in copepod nauplii. *PLoS ONE* **7**, e47486. (doi:10.1371/journal.pone.0047486)
25. Bradley CJ, Strickler JR, Buskey EJ, Lenz PH. 2013 Swimming and escape behavior in two species of calanoid copepods from nauplius to adult. *J. Plankton Res*. **35**, 49–65. (doi:10.1093/Plankt/Fbs088)
26. Moyse J. 1984 Some observations on the swimming and feeding of the nauplius larvae of *Lepas pectinata* (Cirripedia, Crustacea). *Zool. J. Linn. Soc. Lond*. **80**, 323–336. (doi:10.1111/J.1096-3642.1984.Tb01981.X)
27. Wadhwa N, Andersen A, Kiørboe T. 2014 Hydrodynamics and energetics of jumping copepod nauplii and copepodids. *J. Exp. Biol*. **217**, 3085–3094. (doi:10.1242/Jeb.105676)